

# General Carrier Transport Picture for Organic Semiconductors: A Nearly Exact TD-MPS Study on the Nonlocal Electron-Phonon Couplings

Weitang Li, Jiajun Ren, and Zhigang Shuai\*

*MOE Key Laboratory of Organic OptoElectronics and Molecular Engineering,*

*Department of Chemistry, Tsinghua University,*

*Beijing 100084, People's Republic of China*

## Abstract

The role of nonlocal electron-phonon couplings (EPC) in organic semiconductors has been the center of interest recently. Several irreconcilable scenarios coexist for the description of the nonlocal EPC, such as phonon-assisted (PA) transport, transient localization (TL), and band-like (BL) transport. In this Letter, we present a nearly exact numerical study for the carrier mobility of the one-dimensional Holstein-Peierls model using finite temperature time-dependent matrix product states approach. We are able to locate the PA, TL and BL regimes as a function of the electronic coupling ( $V$ ) and the nonlocal EPC ( $\Delta V$ ). The distinct transport behaviors with respect to EPC are analyzed by carrier mobility, mean free path, optical conductivity and one-particle spectral function. We have also identified an “intermediate regime” where none of the established pictures applies, and the generally perceived hopping regime is found to be at a very limited end in the proposed general paradigm.

## INTRODUCTION

The last two decades have witnessed the rapid development of high-mobility crystalline organic semiconductors [1–3]. The first proposition of using Marcus’ semiclassical hopping model coupled with density functional theory to design high mobility molecules has been very successful and gained extreme popularity [4]. It can be regarded as strong local electron-phonon coupling (EPC) limit, which was later improved by considering quantum nuclear effect and delocalization effect [5, 6], through which, isotope effect is found to be always negative and the dynamic disorder does not play appreciable role with some experimental supports [7–10]. However, such local EPC picture is challenged by the recently established transient localization (TL) model which invokes nonlocal EPC [11–14]. In due course, the molecular design principles derived from TL such as suppressing intermolecular vibration, which are quite different from the local picture, have proved successful in a number of experiments [15, 16]. The applicability of the TL picture, nevertheless, is restricted to the regime of moderate electronic coupling (transfer integral)  $V$  and strong nonlocal EPC. Since EPC is a complicated many-body problem, it is highly desirable to present a general transport picture taking both local and nonlocal EPC into considerations in a rigorous way, instead of uncontrolled approximations.

Many recent efforts have been devoted to developing approximate methods that are able to portray a broader parameter space, including the band-like (BL) conduction regime [17, 18]. Besides, unlike in the case of Holstein model in which it is beyond doubt that local EPC represents an obstacle for carrier diffusion [19–21], how nonlocal EPC affects mobility does not have a definitive answer and the interplay between the local and nonlocal EPC is unclear. Early theoretical treatments for carrier mobility in crystalline organic semiconductors such as the Munn-Silbey approach and the polaron transformation often reach to the conclusion that the nonlocal EPC leads to phonon-assisted (PA) transport and enhances mobility [22, 23], in sheer contrast with the basic starting point of the TL scenario. The findings of several numerical studies on the carrier mobility of organic semiconductors also contradict with the TL theory [8, 24]. In principle, PA, TL and BL are all possible mechanisms for charge transport with nonlocal EPC, valid at their respective parameter regimes, yet a universal theoretical treatment for the role of nonlocal EPC is not available due to the complex many-body interaction.

In this Letter, we present the first nearly exact study of the charge transport mechanism in the Holstein-Peierls model using the time dependent finite temperature matrix product state (MPS) formalism [25, 26]. By studying EPC effect on the carrier mobility, mean free path, optical conductivity and one-particle spectral function, we have for the first time located the PA, TL and BL regimes simultaneously on the transfer integral - nonlocal EPC strength plane. We have also identified an intermediate regime where none of the existing pictures is truly applicable, as a generalization of the hopping-band crossover in the Holstein model.

## METHODOLOGY

We take the following one-dimensional Holstien-Peierls model with nearest-neighbour interaction and periodic boundary condition:

$$\begin{aligned}
\hat{H} &= \hat{H}_e + \hat{H}_{\text{ph}} + \hat{H}_{\text{e-ph}} \\
\hat{H}_e &= -V \sum_n (c_{n+1}^\dagger c_n + c_n^\dagger c_{n+1}) \\
\hat{H}_{\text{ph}} &= \sum_{n,m} \omega_m b_{n,m}^\dagger b_{n,m} + \sum_n \omega_\theta b_{n,\theta}^\dagger b_{n,\theta} \\
\hat{H}_{\text{e-ph}} &= \sum_{n,m} g_{m,\text{I}} \omega_m (b_{n,m}^\dagger + b_{n,m}) c_n^\dagger c_n \\
&\quad + \sum_n g_{\theta,\text{II}} \omega_\theta (b_{n,\theta}^\dagger + b_{n,\theta}) (c_{n+1}^\dagger c_n + c_n^\dagger c_{n+1})
\end{aligned} \tag{1}$$

where  $c^\dagger$  ( $c$ ) and  $b^\dagger$  ( $b$ ) are the creation (annihilation) operator for electron and phonon respectively, and  $V$  is the intermolecular electronic coupling or transfer integral.  $\omega_m$  and  $g_{m,\text{I}}$  are the frequency and the dimensionless EPC constant of the  $m$ th intramolecular vibration mode.  $\omega_\theta$  and  $g_{\theta,\text{II}}$  are the intermolecular vibration counterparts.  $\hbar$  is set to 1. The thermal fluctuation  $\Delta V$  is related to intermolecular coupling constant  $g_{\theta,\text{II}}$  by [27]:

$$\Delta V = g_{\theta,\text{II}} \omega_\theta \sqrt{\coth \frac{\omega_\theta}{2k_B T}} \tag{2}$$

In order to elucidate how nonlocal EPC affects charge transport at different transport regimes we focus on the role of electronic coupling  $V$  and nonlocal EPC constant  $g_{\theta,\text{II}}$  (or equivalently  $\Delta V$  at a given  $T$ ). Other parameters are fixed through out this paper unless otherwise specified with values drawn from representative organic semiconductors. In organic semiconductors, the most common values of  $V$  and  $\Delta V$  range from 10 meV to 150 meV

and from 10 meV to 60 meV, respectively [28–30]. The intramolecular vibration frequency  $\omega_m$  and local EPC constant  $g_{m,I}$  are taken from our previous DFT calculations for rubrene and the total  $3N - 6$  normal vibration modes are reduced to 4 effective modes [6, 21], namely  $\omega_m = 26$  meV, 124 meV, 167 meV and 198 meV, with the corresponding dimensionless  $g_{m,I}$  0.83, 0.26, 0.34 and 0.37, respectively. The intermolecular vibration frequency  $\omega_\theta$  is set to be  $50 \text{ cm}^{-1}$  (6.2 meV) as commonly adopted in literature [13, 17, 31].

The carrier mobility is obtained via the Kubo formula [32]:

$$\mu = \frac{1}{k_B T e_0} \int_0^\infty \langle \hat{j}(t) \hat{j}(0) \rangle dt = \frac{1}{k_B T e_0} \int_0^\infty C(t) dt \quad (3)$$

where for the Holstein-Peierls Hamiltonian Eq. 1 the current operator  $\hat{j}$  takes the form:

$$\hat{j} = \frac{e_0 R}{i} \sum_n \left[ -V + g_{\theta,II} \omega_\theta (b_{n,\theta}^\dagger + b_{n,\theta}) \right] (c_{n+1}^\dagger c_n - c_n^\dagger c_{n+1}) \quad (4)$$

Here  $R$  is the intermolecular distance and is set to  $7.2 \text{ \AA}$  as in the case of rubrene crystal. No artificial broadening is applied to  $C(t)$  and we resort to a more strict model with 9 intramolecular modes for the convergence of  $C(t)$  when necessary. Lying at the heart of our calculation is the evaluation of the current-current correlation function  $C(t) = \langle \hat{j}(t) \hat{j}(0) \rangle$ , which is achieved by the time-dependent MPS formalism [21, 25, 26]. In most of our simulations, the number of molecules in the periodic one-dimensional chain is 21 and the virtual bond dimension is 80. More details on the model with 9 intramolecular modes, the algorithm for the calculation of  $C(t)$ , as well as numerical convergence check on MPS parameters are included in the supplementary material.

## RESULTS AND DISCUSSION

Firstly, we analyze the role of local and nonlocal EPC on different parameter regimes by comparing the mobility calculated based on the Holstein-Peierls model ( $\mu_{\text{H-P}}$ ) with the mobility calculated based on pure Holstein model ( $\mu_{\text{H}}$ ) and pure Peierls model ( $\mu_{\text{P}}$ ) at 300 K. We have also included the mobility derived from Matthiessen’s rule ( $1/\mu_{\text{M}} = 1/\mu_{\text{H}} + 1/\mu_{\text{P}}$ ), presumably valid in the BL regime. The overall results are shown in Fig. 1. When  $V = 5$  meV,  $\mu_{\text{H-P}}$  is generally higher than  $\mu_{\text{H}}$ , which implies that nonlocal EPC is beneficial to charge transport. This is considered to be a signature of the PA picture. However, this behavior quickly vanishes as  $V$  increases from 5 meV to 20 meV. At intermediate range

of  $V$ , e.g. from 45 meV to 120 meV,  $\mu_{\text{H-P}}$  could be higher than  $\mu_{\text{P}}$  for larger  $\Delta V$ . That local EPC could enhance instead of reduce mobility is quite counter-intuitive. Such unusual behavior can be best understood by TL picture, in which the quantum coherent interference responsible for Anderson localization can be damaged or destroyed by local EPC as the dissipation force. In addition, the “band width narrowing” caused by local EPC could allow the carrier to thermally access much delocalized states [17]. These lead to the local EPC enhanced mobility. Upon further increasing  $V$  to 150 meV, the TL scenario also becomes less significant. Instead, it is found that  $\mu_{\text{M}}$  coincides with  $\mu_{\text{H-P}}$  remarkably well, serving as an evidence for band-like transport. However,  $\mu_{\text{M}} \approx \mu_{\text{H-P}}$  alone is not a sufficient condition for band-like transport, and we additionally employ the Mott-Ioffe-Regel limit for the determination of the BL regime. The carrier mean free path  $l_{\text{mfp}}$  is estimated as  $l_{\text{mfp}} = v\tau$  with the group velocity  $v$  and relaxation time  $\tau$  evaluated by [33]:

$$\begin{aligned} v &= \sqrt{\langle \hat{j}(0)\hat{j}(0) \rangle} / e_0 \\ \tau &= \int_0^\infty \left| \frac{\text{Re } C(t)}{\text{Re } C(0)} \right| dt. \end{aligned} \quad (5)$$

And the calculated  $l_{\text{mfp}}$  in the  $(V, \Delta V)$  plane at 300 K is shown in Fig. 2a. The overall tendency of  $l_{\text{mfp}}$  matches well with the carrier mobility of the Holstein-Peierls model  $\mu_{\text{H-P}}$  in Fig. 1. The region where  $l_{\text{mfp}} > R$  is colored with blue in Fig. 2a and it lies within the large  $V$ , small  $\Delta V$  limit, in agreement with common perception. Another possible criteria for BL conduction is the appearance of Drude-like peak (DLP) in the per carrier optical conductivity:

$$\frac{\sigma(\omega)}{ne_0} = \frac{1 - e^{-\omega/k_B T}}{\omega} \int_0^\infty C(t) e^{i\omega t} dt \quad (6)$$

which is illustrated in Fig. 2b. In the case of  $V = 150$  meV without nonlocal EPC, a broad DLP appears near  $\omega = 0$ . Upon adding a small amount of nonlocal EPC, the DLP becomes invisible. However, the optical conductivity is still significantly different from the  $\Delta V = 60$  meV cases, in which a localization peak at  $\omega \approx 200$  meV characteristic for the TL regime [18] is present.

To further analyze the charge transport properties in the regimes implied by Fig. 1 and Fig. 2, we calculated the momentum resolved one-particle spectral function:

$$A(k, \omega) = -\frac{1}{L\pi} \sum_{mn} e^{ikR(m-n)} \int_0^\infty \langle a_m(t) a_n^\dagger \rangle e^{i\omega t} dt \quad (7)$$

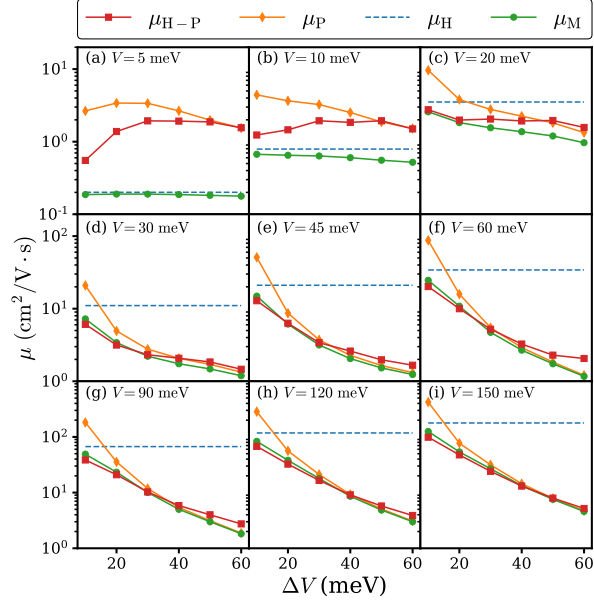


FIG. 1. Carrier mobility at 300 K calculated based on the Holstein-Peierls model ( $\mu_{H-P}$ ), Holstein model ( $\mu_H$ ), Peierls model ( $\mu_P$ ) and Matthiessen's rule ( $\mu_M$ ) with various electronic coupling  $V$  and transfer integral fluctuation  $\Delta V$ . Other parameters relevant to the carrier mobility such as local EPC constants are fixed with values taken from rubrene. The parameters for the Holstein (Peierls) model is the same with that of Holstein-Peierls model except that the nonlocal (local) EPC is left out.

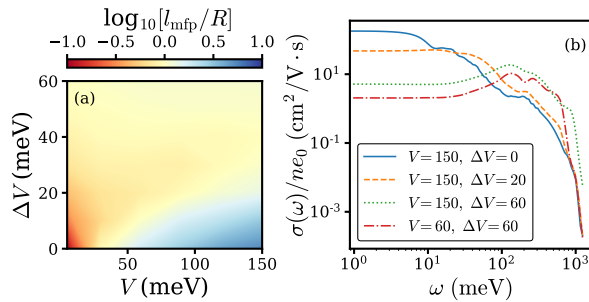


FIG. 2. (a) Carrier mean free path  $l_{mfp}/R$  at 300 K for the Holstein-Peierls model at various transfer integral  $V$  and transfer integral fluctuation  $\Delta V$ . In the blue region the carrier mean free path exceeds the lattice constant  $R$ . (b) Per carrier optical conductivity of the Holstein-Peierls model at various transfer integral  $V$  and transfer integral fluctuation  $\Delta V$ .

for nine sets of representative parameters at 300 K in Fig. 3. A Lorentzian broadening with  $\eta = 5$  meV is applied for a smooth spectra. When  $V = 5$  meV and  $\Delta V = 10$  meV (Fig. 3a), the spectral function exhibits dispersionless bound states separated by the intramolecular vibration frequencies  $\omega_m$ , which marks the formation of small polaron. On the contrary, when  $V = 150$  meV and  $\Delta V = 10$  meV (Fig. 3c) an intense quasiparticle peak is observed near  $k = 0$  and the overall shape of the spectra resembles the dispersion of free electron  $E(k) = -2V \cos kR$ . In the TL regime represented by  $V = 60$  meV and  $\Delta V = 60$  meV (Fig. 3e) the signature of either small polaron or delocalized state is almost completely smeared out. In combination with the limited carrier mean free path in this regime, it can be deduced that the charge carrier is localized by nonlocal EPC instead of local EPC. The same “blurred” spectral function is observed for other sets of typical parameters in the TL regime (Fig. 3d, f). With moderate  $V$  and  $\Delta V$  shown in Fig. 3g, the spectra function exhibits none of the typical features described above. Namely, although the spectral function does not manifest the formation of small polaron or delocalized states, the peak intensity is still strong enough to be discernible from the TL regimes cases (Fig. 3d, e, f). In the absence of the local EPC (Fig. 3h, i), the quasiparticle peak have more intensity, implying the disruption of quantum coherent with the addition of local EPC. Combined with the mobility data shown in Fig. 1, it can be inferred that in the TL regime, the effect of the disruption is to alleviate the localization caused by nonlocal EPC, leading to increased mobility (Fig. 3e, h), while in the BL regime, on the contrary, the disruption scatters charge carrier and reduces mobility (Fig. 3c, i). The horizontal peak at the center of the band in Fig. 3h is a result of the pure nonlocal EPC in the Peierls model and is expected to vanish upon the inclusion of infinitesimal local EPC [34].

Based on the EPC effect on the carrier mobility, the mean free path, the optical conductivity and the one-particle spectral function, we are able to sketch a schematic “regime diagram” for the charge transport mechanisms as shown in Fig. 4. The PA regime, TL regime and BL regime are primarily determined by  $\mu_{\text{H-P}} > \mu_{\text{H}}$ ,  $\mu_{\text{H-P}} \geq \mu_{\text{P}}$  and  $l_{\text{mfp}} > R$  respectively, with other observations serve as supportive evidence of the judgement. More specifically, the localization peak in optical conductivity at large  $\Delta V$  signifies TL transport, and the BL regime is confirmed by the appearance of DLP as well as sharp quasiparticle peak in the spectral function. The regime for the TL scenario is much larger than the parameter regime proposed by the original authors. In their formulation local EPC is completely

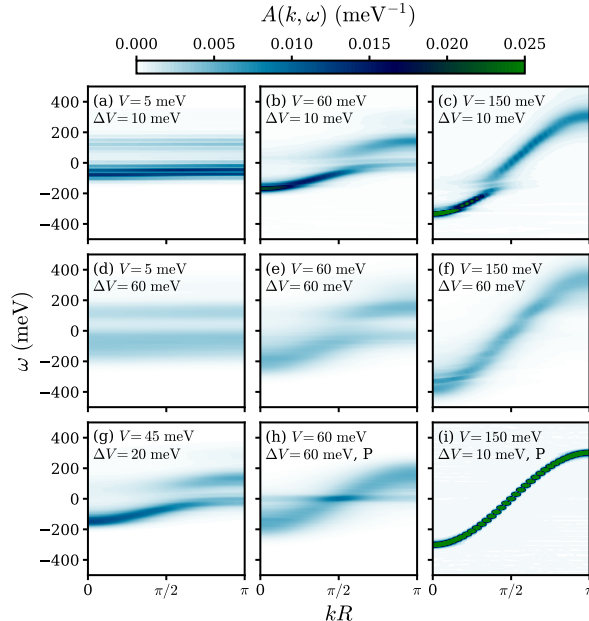


FIG. 3. Spectral function at 300 K for the Holstein-Peierls model [(a) to (g)] and the pure Peierls model [(h) and (i)]. Panel (h) and (i) has the same parameter with panel (e) and (c) respectively except that in Panel (h) and (i) the local EPC is left out.

ignored [11, 35], and thus the validity of TL has been an open question in relatively small  $V$  regime, where the effect of local EPC is considered to be non-negligible. Thanks to the nearly exact MPS method, we have for the first time recognized the boundary of the TL picture toward small  $V$  limit, which lies roughly between 10 meV to 20 meV. On this  $(V, \Delta V)$  plane we are also able to identify an “intermediate” regime that lies among the PA regime, TL regime and TL regime. If the appearance of DLP is chosen to determine the BL regime then a larger intermediate regime is expected. In this regime,  $\mu_{\text{H-P}}$  is significantly lower than both  $\mu_{\text{H}}$  and  $\mu_{\text{P}}$ , and the carrier mean free path is still less than lattice constant, forbidding the band description. In fact, for the pure Holstein model case ( $\Delta V = 0$ ), the intermediate regime simply degenerates into the canonical hopping-band crossover. The grey arrows in Fig 4 indicate the shift of the boundaries upon increasing local EPC and the supportive data is included in the supplementary material. To provide a rough intuition of the distribution of parameters for realistic organic semiconductors on this  $(V, \Delta V)$  plane, in Fig. 4 we have also marked the value of  $V$  and  $\Delta V$  for several common organic semiconductors using reported values from recent literature [29]. These materials are pMSB, pyrene, naphthalene, perylene, anthracene, DATT, rubrene and pentacene from left to right. We note that the colors at the

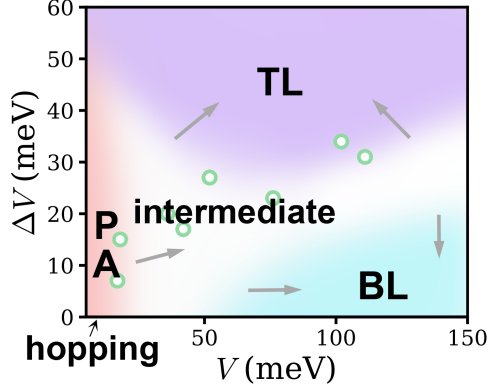


FIG. 4. A schematic “regime diagram” showing the PA (phonon assisted transport) regime, TL (transient localization) regime, BL (band-like) regime and intermediate regime on the  $(V, \Delta V)$  plane for the carrier mobility of the Holstein-Peierls model. The hopping regime is achieved in the  $\Delta V = 0$  limit of the PA regime. Grey arrows show qualitatively the shift of the boundaries when local EPC increases. The green dots represent the parameters of several common organic semiconductors.

location of the markers do not represent a prediction of the charge transport mechanism for the corresponding materials because the materials do not necessarily share the same local EPC coupling strength, transport network and intermolecular vibration frequency with the parameters used in this work.

## CONCLUSION

In this Letter, we present the first nearly exact theoretical study of the carrier mobility in Holstein-Peierls model with parameters relevant to organic semiconductors. By carefully investigating the effect of both local and nonlocal EPCs on the carrier mobility  $\mu$ , mean free path  $l_{\text{mfp}}$ , per carrier optical conductivity  $\frac{\sigma(\omega)}{ne_0}$  and one-particle spectral function  $A(k, \omega)$ , we are able to identify the PA regime, TL regime and BL regime on the  $(V, \Delta V)$  plane. The PA regime features  $\mu_{\text{H-P}} > \mu_{\text{H}}$ , short  $l_{\text{mfp}}$ , and narrow bound states in the spectral function. The TL regime features  $\mu_{\text{H-P}} \geq \mu_{\text{P}}$ , intermediate  $l_{\text{mfp}}$ , localization peak in optical conductivity and a “smeared out” spectral function. And the BL regime features  $\mu_{\text{H-P}} \approx \mu_{\text{M}}$ , large  $l_{\text{mfp}}$ , DLP in optical conductivity and sharp quasiparticle peak in the spectral function. The semiclassical Marcus hopping regime is found to be around the corner of small  $V$  and

$\Delta V$ . Furthermore, some of the parameters in the  $(V, \Delta V)$  plane are recognized to lie in an intermediate regime which does not exhibit the typical features described above, and this regime can be considered as a generalization of the hopping-band crossover regime in the Holstein model. It should be noted that the localization effect due to static disorder is not considered here, which deserves further investigation.

This work is supported by the National Natural Science Foundation of China (NSFC) through the project “Science Center for Luminescence from Molecular Aggregates (SCELMA)” Grant Number 21788102, as well as by the Ministry of Science and Technology of China through the National Key R&D Plan Grant Number 2017YFA0204501. J.R. is also supported by the NSFC via Grant Number 22003029.

---

\* zgshuai@mail.tsinghua.edu.cn

- [1] V. Podzorov, E. Menard, A. Borissov, V. Kiryukhin, J. A. Rogers, and M. E. Gershenson, *Phys. Rev. Lett.* **93**, 086602 (2004).
- [2] V. Podzorov, E. Menard, J. A. Rogers, and M. E. Gershenson, *Phys. Rev. Lett.* **95**, 226601 (2005).
- [3] C. Mitsui, T. Okamoto, M. Yamagishi, J. Tsurumi, K. Yoshimoto, K. Nakahara, J. Soeda, Y. Hirose, H. Sato, A. Yamano, T. Uemura, and J. Takeya, *Adv. Mater.* **26**, 4546 (2014).
- [4] J. L. Brédas, J. P. Calbert, D. A. da Silva Filho, and J. Cornil, *Proc. Natl. Acad. Sci.* **99**, 5804 (2002).
- [5] G. Nan, X. Yang, L. Wang, Z. Shuai, and Y. Zhao, *Phys. Rev. B* **79**, 115203 (2009).
- [6] Y. Jiang, X. Zhong, W. Shi, Q. Peng, H. Geng, Y. Zhao, and Z. Shuai, *Nanoscale Horiz.* **1**, 53 (2016).
- [7] Y. Jiang, Q. Peng, H. Geng, H. Ma, and Z. Shuai, *J. Phys. Chem. Lett.* **17**, 3273 (2015).
- [8] L. Wang, Q. Li, Z. Shuai, L. Chen, and Q. Shi, *Phys. Chem. Chem. Phys.* **12**, 3309 (2010).
- [9] X. Ren, M. J. Bruzek, D. A. Hanifi, A. Schulzetenberg, Y. Wu, C.-H. Kim, Z. Zhang, J. E. Johns, A. Salleo, S. Fratini, A. Troisi, C. J. Douglas, and C. D. Frisbie, *Adv. Electron. Mater.* **3**, 1700018 (2017).
- [10] A. D. Platt, M. J. Kendrick, M. Loth, J. E. Anthony, and O. Ostroverkhova, *Phys. Rev. B* **84**, 235209 (2011).

- [11] S. Fratini and S. Ciuchi, *Phys. Rev. Lett.* **103**, 266601 (2009).
- [12] S. Fratini, D. Mayou, and S. Ciuchi, *Adv. Funct. Mater.* **26**, 2292 (2016).
- [13] S. Fratini, S. Ciuchi, D. Mayou, G. T. de Laissardière, and A. Troisi, *Nat. Mater.* **16**, 998 (2017).
- [14] G. Schweicher, G. D'Avino, M. T. Ruggiero, D. J. Harkin, K. Broch, D. Venkateshvaran, G. Liu, A. Richard, C. Ruzié, J. Armstrong, A. R. Kennedy, K. Shankland, K. Takimiya, Y. H. Geerts, J. A. Zeitler, S. Fratini, and H. Sirringhaus, *Adv. Mater.* **31**, 1902407 (2019).
- [15] T. Kubo, R. Häusermann, J. Tsurumi, J. Soeda, Y. Okada, Y. Yamashita, N. Akamatsu, A. Shishido, C. Mitsui, T. Okamoto, S. Yanagisawa, H. Matsui, and J. Takeya, *Nat. Commun.* **7**, 11156 (2016).
- [16] S. Illig, A. S. Eggeman, A. Troisi, L. Jiang, C. Warwick, M. Nikolka, G. Schweicher, S. G. Yeates, Y. Henri Geerts, J. E. Anthony, and H. Sirringhaus, *Nat. Commun.* **7**, 10736 (2016).
- [17] J. H. Fetherolf, D. Golež, and T. C. Berkelbach, *Phys. Rev. X* **10**, 021062 (2020).
- [18] S. Fratini and S. Ciuchi, *Phys. Rev. Research* **2**, 013001 (2020).
- [19] T. Holstein, *Ann. Phys.* **8**, 325 (1959).
- [20] A. S. Mishchenko, N. Nagaosa, G. De Filippis, A. de Candia, and V. Cataudella, *Phys. Rev. Lett.* **114**, 146401 (2015).
- [21] W. Li, J. Ren, and Z. Shuai, *J. Phys. Chem. Lett.* **11**, 4930 (2020).
- [22] R. Munn and R. Silbey, *J. Chem. Phys.* **83**, 1854 (1985).
- [23] K. Hannewald, V. Stojanović, J. Schellekens, P. Bobbert, G. Kresse, and J. Hafner, *Phys. Rev. B* **69**, 075211 (2004).
- [24] W. Zhang, X. Zhong, and Y. Zhao, *J. Phys. Chem. A* **116**, 11075 (2012).
- [25] U. Schollwöck, *Ann. Phys.* **326**, 96 (2011).
- [26] S. Paeckel, T. Köhler, A. Swoboda, S. R. Manmana, U. Schollwöck, and C. Hubig, *Ann. Phys.* **411**, 167998 (2019).
- [27] V. Coropceanu, R. S. Sánchez-Carrera, P. Paramonov, G. M. Day, and J.-L. Brédas, *J. Phys. Chem. C* **113**, 4679 (2009).
- [28] A. Landi and A. Troisi, *J. Phys. Chem. C* **122**, 18336 (2018).
- [29] S. Giannini, A. Carof, M. Ellis, H. Yang, O. G. Ziegler, S. Ghosh, and J. Blumberger, *Nat. Commun.* **10**, 3843 (2019).
- [30] S. Fratini, M. Nikolka, A. Salleo, G. Schweicher, and H. Sirringhaus, *Nat. Mater.* **19**, 491

(2020).

- [31] A. Troisi, *Adv. Mat.* **19**, 2000 (2007).
- [32] G. D. Mahan, *Many-Particle Physics* (Springer, US, 2000).
- [33] N. Prodanović and N. Vukmirović, *Phys. Rev. B* **99**, 104304 (2019).
- [34] G. Theodorou and M. H. Cohen, *Phys. Rev. B* **13**, 4597 (1976).
- [35] S. Ciuchi and S. Fratini, *Phys. Rev. B* **86**, 245201 (2012).

# Supplementary Material for “General Carrier Transport Picture for Organic Semiconductors: A Nearly Exact TD-MPS Study on the Nonlocal Electron-Phonon Couplings”

Weitang Li, Jiajun Ren, and Zhigang Shuai\*

MOE Key Laboratory of Organic Optoelectronics and Molecular Engineering,  
Department of Chemistry, Tsinghua University, Beijing 100084, People’s Republic of China

## CALCULATION OF CARRIER MOBILITY AND SPECTRAL FUNCTION

The evaluation of the current-current correlation function  $C(t) = \langle \hat{j}(t) \hat{j}(0) \rangle$  is performed by TD-MPS through imaginary and real time propagation. The finite temperature effect is taken into account through thermal field dynamics, also known as the purification method [1, 2]. The thermal equilibrium density matrix of any mixed state in physical space  $P$  can be expressed as a partial trace over an enlarged Hilbert space  $P \otimes Q$ , where  $Q$  is an auxiliary space chosen to be a copy of  $P$ . The thermal equilibrium density operator can then expressed as a partial trace of the pure state  $|\Psi_\beta\rangle$  in the enlarged Hilbert space over the  $Q$  space:

$$\hat{\rho}_\beta = \frac{e^{-\beta\hat{H}}}{Z} = \frac{\text{Tr}_Q |\Psi_\beta\rangle \langle \Psi_\beta|}{\text{Tr}_{PQ} |\Psi_\beta\rangle \langle \Psi_\beta|} \quad (1)$$

and the pure state  $|\Psi_\beta\rangle$  represented as an MPS is obtained by the imaginary time propagation from the locally maximally entangled state  $|I\rangle = \sum_i |i\rangle_P |i\rangle_Q$  to  $\beta/2$ :

$$|\Psi_\beta\rangle = e^{-\beta\hat{H}/2} |I\rangle. \quad (2)$$

To calculate  $C(t)$ ,  $|\Psi_\beta\rangle$  and  $\hat{j}(0)|\Psi_\beta\rangle$  are propagated in real time to obtain  $e^{-i\hat{H}t} |\Psi_\beta\rangle$  and  $e^{-i\hat{H}t} \hat{j}(0) |\Psi_\beta\rangle$  and then  $C(t)$  is calculated by:

$$C(t) = \langle \Psi_\beta | e^{i\hat{H}t} \hat{j}(0) e^{-i\hat{H}t} \hat{j}(0) | \Psi_\beta \rangle / Z. \quad (3)$$

Here the current operator  $\hat{j}(0)$  is represented as an MPO and inner-product for  $|\Psi_\beta\rangle$  includes tracing over both  $P$  space and  $Q$  space. The construction of the MPOs is performed in an automatic and optimal fashion through our recently proposed algorithm [3]. In principle, both imaginary and real time propagation can be carried out by any time evolution methods available to TD-MPS [4]. In this work, we use the time-dependent variational principle based projector splitting time evolution scheme [5, 6], which is found to be relatively efficient and accurate combined with graphic processing unit (GPU) in our recent work [7].

Next we present details on our MPS time evolution parameters and respective numerical convergence verification. The calculation of  $C(t)$  involves three sets of time evolution: the imaginary time evolution for  $|\Psi_\beta\rangle$ , real time evolution for  $e^{-i\hat{H}t} |\Psi_\beta\rangle$  and real time evolution for  $e^{-i\hat{H}t} \hat{j}(0) |\Psi_\beta\rangle$ . For efficient calculation, we use different bond dimensions for the three time evolutions. More specifically, time evolutions for  $|\Psi_\beta\rangle$  and  $e^{-i\hat{H}t} |\Psi_\beta\rangle$  share the same bond dimension  $iM$ , and the time evolution for  $e^{-i\hat{H}t} \hat{j}(0) |\Psi_\beta\rangle$  has the bond dimension  $M$ . Other important parameters relevant to the time evolution includes the number of molecules in the periodic one dimensional chain  $N$ , the number of truncated harmonic oscillator eigenbasis for the intermolecular vibration  $l$ , and time evolution step  $dt$ . For most of our calculations,  $iM$ ,  $M$ ,  $N$ ,  $l$  and  $dt$  are set to 64, 80, 21, 40, 50 respectively, and numerical convergence in the large transfer integral  $V = 150$  meV and strong nonlocal EPC coupling  $\Delta V = 60$  meV limit is shown in Fig. 1. This is considered to be a set of challenging parameter due to the strong EPC and non-trivial physical behavior as discussed in the main text.

We note, however, that a fixed set of MPS parameters is not sufficient for converged result over the whole  $(V, \Delta V)$  plane explored in the main text, and we in fact adjust the MPS parameters accordingly to ensure that numerically exact result is obtained. We show in Fig. 2 the numerical convergence check for the pure Holstein model at  $V = 150$  meV. In this regime,  $C(t)$  decays in a slower rate, requiring longer evolution time and consequently larger virtual bond dimension. Besides, the high mobility also demands larger system size in order to eliminate the finite size effect. So in the bottom-right corner of the  $(V, \Delta V)$  plane we have carefully checked  $M$  and  $N$  and use values larger than 80 and 21 for  $M$  and  $N$  when necessary.

The evaluation of the one-particle spectral function  $A(k, \omega)$  further takes advantage of the fact that the thermal equilibrium state is a zero-electron state. In this case, the thermal field dynamics algorithm can be reformulated to reduce computational cost [8, 9]. For the calculation of  $A(k, \omega)$  we use a system size of 64 and virtual bond dimension of 64. We benchmark our

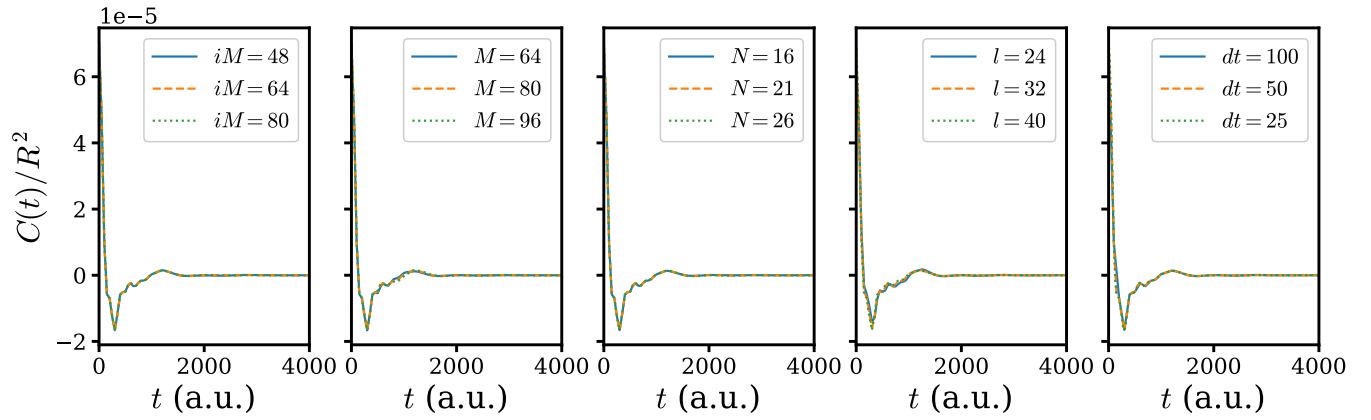


FIG. 1. Numeric convergence check for  $C(t)$  of the Holstein-Peierls model in the  $V = 150$  meV and  $\Delta V = 60$  meV case.

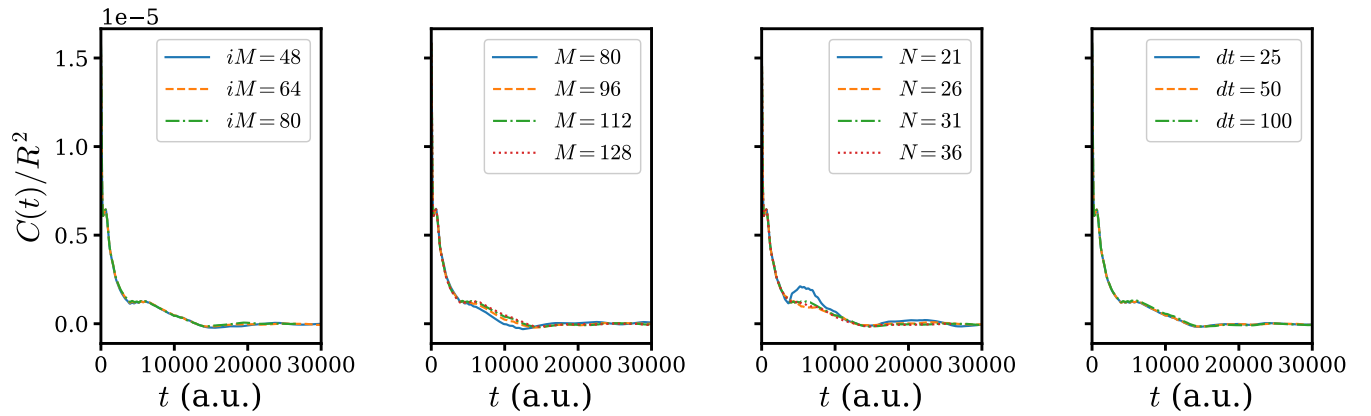


FIG. 2. Numeric convergence check for  $C(t)$  of the pure Holstein model in the  $V = 150$  meV case.

algorithm on a pure Holstein model with a single vibration mode at zero temperature, and our result (Fig. 3) is in quantitative agreement with exact diagonalization method [10].

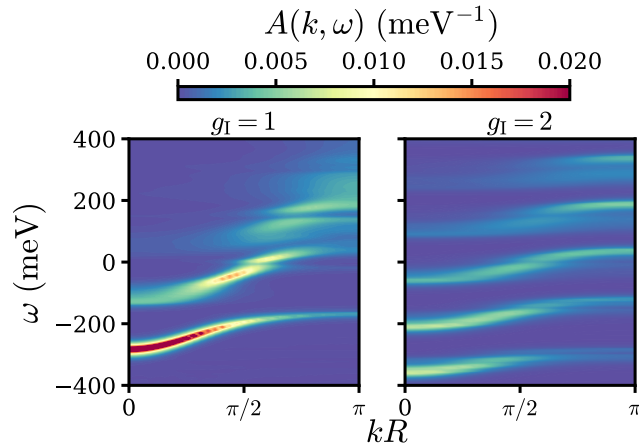


FIG. 3. Spectral function at zero temperature for the single-mode Holstein model. The parameters are:  $V = 100$ , meV,  $\omega = 150$  meV and a Lorentzian broadening with  $\eta = 10$  meV.

## THE NUMBER OF INTRAMOLECULAR VIBRATION MODES

Organic molecules usually contain dozens of atoms and it is common for more than 10 vibrational modes to contribute to local EPC. For simplicity, theoretical studies often reduce the modes into one effective mode [10–12]. However, by taking this approach, the correlation function  $C(t)$  typically exhibits spurious long correlation time which is generally not possible for realistic material. In such cases, an artificial and sometimes arbitrary broadening is usually applied to  $C(t)$  in order to mimic realistic world and determine an absolute value for mobility. In the main text most of our results are reported with a 4-(intramolecular-)mode model and  $C(t)$  generally rapidly decays to zero. But in cases of small  $V$  and  $\Delta V$  we have to further resort to a 9-(intramolecular-)mode model with vibration energy and EPC constant listed in Table I to avoid artificial recurrence. Starting from more than 40 vibrational modes that contribute to local EPC in rubrene crystal obtained by *ab initio* calculation, the 9-mode model is generated by dropping the modes with  $\lambda_m = g_{m,I}^2 \omega_m < 20 \text{ cm}^{-1}$  and adding  $\lambda_m$  of the dropped modes to the closest retained modes, while the 4-mode model is generated in the same way except that the dropping threshold is upraised to  $50 \text{ cm}^{-1}$  [13]. Thus, the 9-mode model and the 4-mode model share the same total reorganization energy  $\sum_m \lambda_m$  and the 9-mode model in principle describes realistic material better than the 4 mode-model.

TABLE I. Vibration energy and local EPC constant of the 9-intramolecular-mode model.

| Mode No.         | 1    | 2    | 3    | 4    | 5    | 6    | 7    | 8    | 9    |
|------------------|------|------|------|------|------|------|------|------|------|
| $\omega_m$ (meV) | 10   | 27   | 78   | 124  | 149  | 167  | 169  | 190  | 198  |
| $g_{m,I}$        | 0.96 | 0.38 | 0.25 | 0.20 | 0.15 | 0.31 | 0.13 | 0.20 | 0.31 |

In Fig. 4 we list the parameters for which we have used the 9-mode model as well as the corresponding correlation functions  $C(t)$ . In Fig. 4(a) and (c) it can be seen that that the artificial recurrence around 6000 a.u. for the 4-mode model is absent in the 9-mode model. On the other hand,  $C(t)$  of the 4-mode model and the 9-mode model agree well in the small  $t$  regime. For the  $V = 5 \text{ meV}$ ,  $\Delta V = 10 \text{ meV}$  case and the  $V = 20 \text{ meV}$ ,  $\Delta V = 0 \text{ meV}$  case shown in Fig. 4(b) and (d),  $C(t)$  for the 4-mode model takes a long time to decay to zero, while  $C(t)$  for the 9-mode model decays to zero in a faster manner.

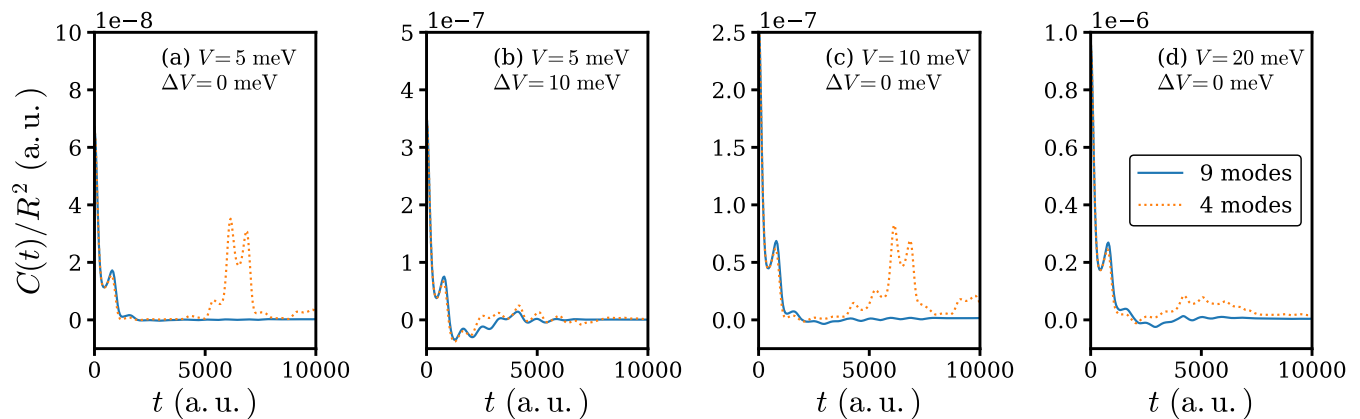


FIG. 4. Comparison of the current-current correlation function  $C(t)$  obtained from the 4-mode model and the 9-mode model.

## PHASE DIAGRAM WITH LARGER LOCAL EPC

In order to investigate how the “phase diagram” presented in the main text evolves with respect to the strength of local EPC, we have further calculated the carrier mobility of the Holstein-Peierls model with stronger local EPC. More specifically, the value of  $g_{m,I}$  is multiplied by  $\sqrt{2}$  so that the respective reorganization energy  $g_{m,I}^2 \omega_m$  is doubled. The results are illustrated in Fig. 5. In the small  $V$  limit shown in Fig. 5(a), the PA mechanism prevails, in agreement with the results in the main text. However, from Fig. 5(b) it can be seen that with enlarged local EPC strength the PA picture remains valid even if  $V$  becomes as large as 20 meV, in contrast to the  $V = 20 \text{ meV}$  results presented in the main text, indicating the expansion of the PAT region. Accordingly, the TL region is diminished, as can be inferred from Fig. 5(c) and (d) by noting that the parameter space in which  $\mu_{\text{H-P}} \geq \mu_{\text{P}}$  is satisfied is smaller than that of the main text.

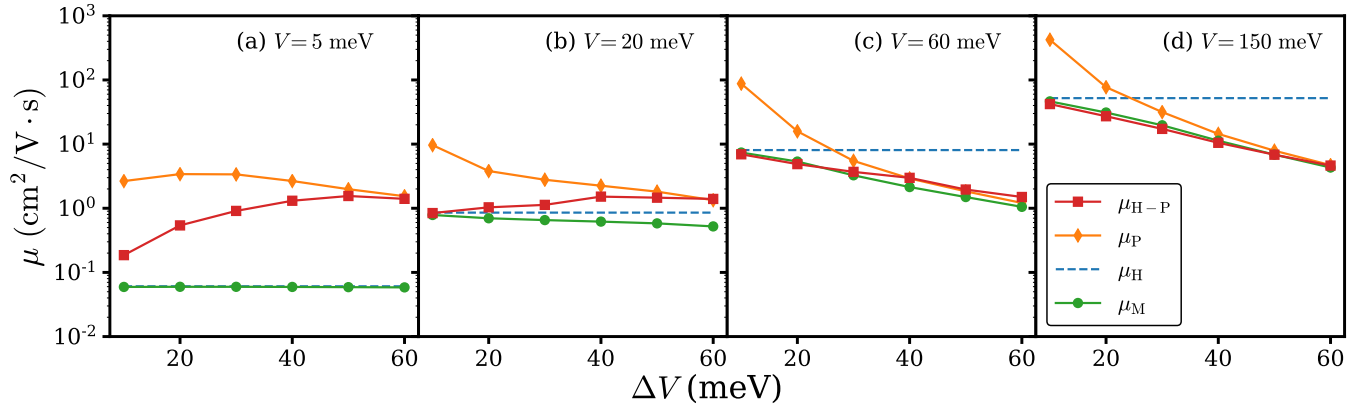


FIG. 5. Carrier mobility at 300 K calculated based on the Holstein-Peierls model ( $\mu_{H-P}$ ), Holstein model ( $\mu_H$ ), Peierls model ( $\mu_P$ ) and Matthiessen's rule ( $\mu_M$ ) with enlarged local EPC at various transfer integral  $V$  and transfer integral fluctuation  $\Delta V$ .

In Fig. 6 we show the carrier mean free path  $l_{\text{mfp}}/R$  as defined in the main text, with increased local EPC strength. When  $V$  is relatively large and  $\Delta V$  is relatively small, namely in the BL regime,  $l_{\text{mfp}}/R$  with increased local EPC strength is generally smaller than that of the original local EPC strength. This observation implies that the BL region in the  $(V, \Delta V)$  plane moves toward the even larger  $V$  area ( $V > 150$  meV).

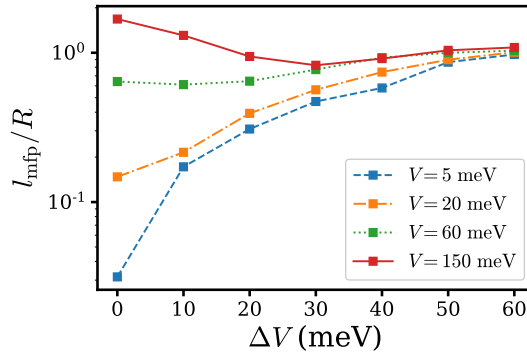


FIG. 6. Carrier mean free path  $l_{\text{mfp}}/R$  at 300 K for the Holstein-Peierls model with enlarged local EPC at various transfer integral  $V$  and transfer integral fluctuation  $\Delta V$ .

\* zgshuai@tsinghua.edu.cn

- [1] A. E. Feiguin and S. R. White, Finite-temperature density matrix renormalization using an enlarged Hilbert space, *Phys. Rev. B* **72**, 220401 (2005).
- [2] U. Schollwöck, The density-matrix renormalization group in the age of matrix product states, *Ann. Phys.* **326**, 96 (2011).
- [3] J. Ren, W. Li, T. Jiang, and Z. Shuai, A general automatic method for optimal construction of matrix product operators using bipartite graph theory, *J. Chem. Phys.* **153**, 084118 (2020).
- [4] S. Paeckel, T. Köhler, A. Swoboda, S. R. Manmana, U. Schollwöck, and C. Hubig, Time-evolution methods for matrix-product states, *Ann. Phys.* **411**, 167998 (2019).
- [5] J. Haegeman, J. I. Cirac, T. J. Osborne, I. Pižorn, H. Verschelde, and F. Verstraete, Time-dependent variational principle for quantum lattices, *Phys. Rev. Lett.* **107**, 070601 (2011).
- [6] J. Haegeman, C. Lubich, I. Oseledets, B. Vandereycken, and F. Verstraete, Unifying time evolution and optimization with matrix product states, *Phys. Rev. B* **94**, 165116 (2016).
- [7] W. Li, J. Ren, and Z. Shuai, Numerical assessment for accuracy and GPU acceleration of TD-DMRG time evolution schemes, *J. Chem. Phys.* **152**, 024127 (2020).
- [8] R. Borrelli and M. F. Gelin, Quantum electron-vibrational dynamics at finite temperature: Thermo field dynamics approach, *J. Chem. Phys.* **145**, 224101 (2016).

- [9] D. Tamascelli, A. Smirne, J. Lim, S. F. Huelga, and M. B. Plenio, Efficient simulation of finite-temperature open quantum systems, *Phys. Rev. Lett.* **123**, 090402 (2019).
- [10] J. H. Fetherolf, D. Golež, and T. C. Berkelbach, A unification of the Holstein polaron and dynamic disorder pictures of charge transport in organic crystals, *Phys. Rev. X* **10**, 021062 (2020).
- [11] K. Hannewald and P. Bobbert, Ab initio theory of charge-carrier conduction in ultrapure organic crystals, *Appl. Phys. Lett.* **85**, 1535 (2004).
- [12] A. Troisi, Prediction of the absolute charge mobility of molecular semiconductors: The case of rubrene, *Adv. Mat.* **19**, 2000 (2007).
- [13] W. Li, J. Ren, and Z. Shuai, Finite-temperature TD-DMRG for the carrier mobility of organic semiconductors, *J. Phys. Chem. Lett.* **11**, 4930 (2020).